nature communications

Article

https://doi.org/10.1038/s41467-025-59403-z

Limited cell-autonomous anticancer mechanisms in long-lived bats

Received: 29 February 2024

Accepted: 22 April 2025

Published online: 03 May 2025

Check for updates

Fathima Athar[1,7], Zhizhong Zheng[1,7], Sebastien Riquier[2], Max Zacher[1], J. Yuyang Lu[1], Yang Zhao[1], Valentin Volobaev[1], Dominic Alcock[2], Alex Galazyuk[3], Lisa Noelle Cooper[3], Tony Schountz[4], Lin-Fa Wang[5], Emma C. Teeling[2], Andrei Seluanov[1,6] ✉ & Vera Gorbunova[1,6] ✉

Several bat species live >20–40 years, suggesting that they possess efficient anti-aging and anti-cancer defenses. Here we investigate the requirements for malignant transformation in primary fibroblasts from four bat species *Myotis lucifugus*, *Eptesicus fuscus*, *Eonycteris spelaea*, and *Artibeus jamaicensis* – spanning the bat evolutionary tree and including the longest-lived genera. We show that bat fibroblasts do not undergo replicative senescence, express active telomerase, and show attenuated SIPs with dampened secretory phenotype. Unexpectedly, unlike other long-lived mammals, bat fibroblasts are readily transformed by two oncogenic "hits": inactivation of p53 or pRb and activation of $HRAS^{G12V}$. Bat fibroblasts exhibit increased *TP53* and *MDM2* transcripts and elevated p53-dependent apoptosis. *M. lucifugus* shows a genomic duplication of *TP53*. We hypothesize that some bat species have evolved enhanced p53 activity as an additional anti-cancer strategy, similar to elephants. Further, the absence of unique cell-autonomous tumor suppressive mechanisms may suggest that in vivo bats may rely on enhanced immunosurveillance.

Bats exhibit diverse lifespans[1,2] with many species showing exceptional longevity. Longevity quotient (LQ) is the ratio of observed maximum longevity to the predicted lifespan normalized to the body size. Across Chiroptera, 65 species have a mean LQ of 3.52. It means that these bats live 3.5 times longer than what is predicted by their body size[3] making them excellent models to investigate adaptations for longevity.

Several studies have analyzed the association of cancer prevalence with life history traits of organisms across phyla[4–7]. Cancer is a multistage process involving the accumulation of genetic and epigenetic mutations in mitotic cells, and the frequency of tumor formation depends on the number of cell divisions over time. Therefore, longer lifespans with more cell divisions, and longer exposure to exo- and endogenous stressors increase cancer incidence[8,9]. However, despite their exceptional lifespans, few to no tumors have been reported in long-lived wild and captive populations of bats[6,10–13]. Several comparative studies have uncovered cell autonomous (determined by intrinsic properties of the cells) and non-cell autonomous (determined by cell microenvironment or cell-cell interactions) adaptations in long-lived species that have anti-cancer functions. These include regulating telomerase activity in large species[14–16], increase in tumor suppressor gene copies in elephants[17–19], decreased non-LTR retrotransposition[20], transposon-triggered innate immune responses for cell clearance[21], enhanced DNA repair in long-lived rodents[22], and regulation of uncontrolled proliferation by unique mechanisms such as early

[1]Department of Biology, University of Rochester, Rochester, NY, USA. [2]School of Biology and Environmental Science, Belfield, University College Dublin, Dublin, Ireland. [3]Department of Anatomy and Neurobiology, Northeast Ohio Medical University, Rootstown, Ohio, USA. [4]Department of Microbiology, Immunology, and Pathology, College of Veterinary Medicine and Biomedical Sciences, Colorado State University, Fort Collins, CO, USA. [5]Programme in Emerging Infectious Diseases, Duke-NUS Medical School, Singapore 169857, Singapore; SingHealth Duke-NUS Global Health Institute, Singapore, Singapore. [6]Department of Medicine, University of Rochester Medical Center, Rochester, NY, USA. [7]These authors contributed equally: Fathima Athar, Zhizhong Zheng. ✉e-mail: Andrei.Seluanov@rochester.edu; Vera.Gorbunova@rochester.edu

contact inhibition in the naked mole rat and massive necrotic cell death in the blind mole rat[23,24].

Bat genomic studies revealed multiple adaptive changes in their immune systems[25–33]. Many of these changes temper inflammation (reviewed in ref. 34), which may have an anticancer effect. In addition, signatures of positive selection were detected in tumor suppressors[35], DNA damage checkpoint and DNA repair pathway genes[25,35], and growth hormones[36]. However, with the exception of a recently published study[37], malignant transformation has not been experimentally investigated in bat primary cells.

The number of oncogenic hits required for malignant transformation in vitro varies by species. Human fibroblasts require 5 mutational hits for malignant transformation, while mouse cells require only 2: inactivation of either pRb or p53 tumor suppressors and activation of the Ras signaling pathway[38]. We previously investigated the numbers of oncogenic hits required for the transformation of multiple rodent species. The number of hits was shown to increase with animal size and lifespan (ranging between 2 in the mouse and 5 in the beaver), reflecting stricter control over cell proliferation in longer-lived and larger-sized species[15].

In the present study, we investigate anti-cancer mechanisms in bats. We use primary wing fibroblasts from four species of bats; the little brown bat (*Myotis lucifugus*) with a maximum lifespan (MLS) of 34 years, the big brown bat (*Eptesicus fuscus*; MLS of 19 years), the cave nectar bat (*Eonycteris spelaea*; MLS of over 8 years; related species *Eidolon helvum* have MLS of 22 years), and the Jamaican fruit bat (*Artibeus jamaicensis*; MLS of 19 years). These species are from four bat families, span both bat suborders, and include the longest-lived genera *Myotis*[39]. *M. lucifugus* and *E. fuscus* are from the family Vespertilionidae, and *A. jamaicensis* is from Phyllostomidae, both lineages are within the suborder Yangochiroptera. *E. spelaea*, from the family Pteropodidae, is placed within the other suborder Yinpterochiroptera. We investigate telomerase activity, number of 'hits' required for malignant transformation, and response to stress-induced premature senescence (SIPS) in bat wing fibroblasts, alongside skin fibroblasts from mice and humans for comparison. Hereafter, we use the word 'bats' to refer to the four species examined in this study. We show that, surprisingly, bat fibroblasts require only 2 oncogenic hits for malignant transformation, which include inactivation of either p53 or pRb pathways and activation of RAS. Furthermore, bat cells exhibit elevated p53 activity and higher p53 transcript levels, which resemble anti-tumor adaptations observed in elephants[17,18].

Results

Primary bat fibroblasts and tissues are positive for telomerase activity

Telomeres in mammals are long tracts of tandem hexameric TTAGGG nucleotide repeats that protect the ends of the chromosomes and usually require a specialized RNA-dependent DNA polymerase, telomerase, to be replicated. Telomerase is repressed in somatic cells of large mammals[14] but is reactivated during tumorigenesis. Hence, suppression of somatic telomerase activity represents a tumor suppressor mechanism that evolves with large body size[40,41]. We used Telomere Repeat Amplification Protocol (TRAP), a PCR-based assay, to test for telomerase activity.

Cell extracts tested by the TRAP assay showed that all four bat species possess telomerase activity in their wing fibroblasts. *M. lucifugus* and *E. fuscus* fibroblasts showed robust telomerase activity when compared to *E. spelaea* and *A. jamaicensis* (Fig. 1a). We also confirmed this by testing several tissues we obtained from two of the bat species. Extracts from lung, spleen, wing, liver, heart, kidney, and brain tissues from *E. fuscus* and *E. spelaea* showed telomerase activity. Within each bat, post-mitotic tissues like the heart and kidney showed lower activity than the lung, liver, spleen, and wing tissues, with the spleen showing the highest activity (Fig. 1b). Telomerase activity in the wing tissue extract of *E. fuscus* was higher than in *E. spelaea*, similar to the observations with their wing fibroblast cultures. Bat wing fibroblasts proliferated continuously in culture and did not show replicative senescence, which is consistent with the presence of active telomerase (Fig. 1c). We then tested telomerase activity in wing fibroblasts from *M. lucifugus* and *E. spelaea* differing by at least 20 population doublings (PDs) (Fig. 1d). We found small to negligible reduction in telomerase activity in fibroblasts differing by 20 PDs from both *M. lucifugus* and *E. spelaea*, suggesting that the telomerase activity is sustained over several cell divisions.

A previous study assessed telomerase expression in blood and wing-punch-derived fibroblast transcriptomes. It hypothesized absence of TERT-mediated telomere maintenance in the long-lived bat *Myotis myotis* (MLS 37 years) given that relative telomere length did not change with age yet there was no evidence of significant TERT expression in the transcriptome data sets examined[1]. We tested wing fibroblast cultures from this population of *Myotis myotis* bats using the TRAP assay and found that fibroblast extracts were positive for telomerase activity (Supplementary Fig. 1e). This suggests that telomere maintenance in *Myotis myotis* also follows canonical telomerase-mediated mechanisms with small-bodied species expressing active telomerase, but without the expected increase in cancer incidence typical of other small-bodied species.

Bat fibroblasts require two oncogenic 'hits' for malignant transformation

Cell-type and species-specific differences have been demonstrated in the number of pathways to be perturbed ("hits") for oncogenic transformation. The number and type of hits required for transformation may provide insights into species-specific inherent barriers to cancer formation in vivo. Human fibroblasts have been shown to require five to six pathways altered, while mice require two oncogenic hits for malignant transformation[38].

We sought to investigate if bat cells possess intrinsic mechanisms that confer resistance to malignant transformation. Wing fibroblasts from three bat species were used: *M. lucifugus*, *E. fuscus*, and *E. spelaea*. Stably transformed fibroblasts were generated by drug selection, expressing SV40 LT (binds and inactivates both p53 and pRb family of proteins) and its mutants - SV40-LT-K1 (inactivates p53 only) and SV40 LT-Δ 434-444 (inactivates pRb family only), each in combination with $HRas^{G12V}$. The combination of $HRas^{G12V}$ with SV40 LT constitutes three hits, while $HRas^{G12V}$ with either of the SV40 LT mutants constitutes two oncogenic hits. Fibroblasts expressing GFP plasmid, SV40 LT-only, or $HRas^{G12V}$-only were used as controls. Exogenous telomerase was not used because all these bat species showed intrinsic telomerase activity in our TRAP assays.

First, we analyzed anchorage-independent growth in soft agar assay. Surprisingly, overexpression of $HRas^{G12V}$ along with either of the mutants of SV40 LT was sufficient for colony formation in all three bat species (Fig. 2a). This suggests that two oncogenic hits -overexpression of HRas and inhibition of either p53 or pRb family of proteins - are sufficient for oncogenic transformation of bat fibroblasts. No colonies formed in controls.

We further tested if transformed fibroblasts can form tumors in the mouse xenograft assay. No tumors formed in mice injected with control cells expressing SV40 LT or GFP only. Fibroblasts transformed with three forms of SV40 LT antigen along with $HRas^{G12V}$ formed tumors in all three bat species, albeit with different tumor growth kinetics (Fig. 2b, c). $HRas^{G12V}$ with SV40 LT (three hits) grew the fastest (Fig. 2c). Overexpression of $HRas^{G12V}$ with either mutant of SV40 LT was sufficient for tumor formation. Thus, just as with laboratory mouse fibroblasts, a minimum of two hits were sufficient to transform bat fibroblasts.

Bat fibroblasts display attenuated Stress-Induced Premature Senescence (SIPS) and instead undergo p53-dependent apoptosis

Stress-induced premature senescence (SIPS) is the premature induction of senescence in cells using exogenous stressors. Two doses of γ-

radiation (10 and 20 Gy) were used to induce SIPs in wing fibroblasts from four species of bats, dermal fibroblasts from humans, and laboratory and wild-caught mice, and the outcomes were compared. Cell proliferation was measured by the BrdU incorporation assay three days post-radiation. Cells from all species underwent cell cycle arrest, with more than 50% reduction in BrdU positive cells at 10 and 20 Gy (Fig. 3a). Day 12 post-radiation, the cells were analyzed for induction of senescence by staining for Senescence-associated β-galactosidase (SA-β-gal). At 10 Gy, about 40–60% senescent cells were observed in human and mice fibroblast cultures. However, the number of senescent cells in *M. lucifugus* and *A. jamaicensis* were four-fold lower (Fig. 3b, c) compared to human cells. We found that the number of senescent cells in *E. fuscus* was similar to mouse at 10 Gy. No interspecies differences in SA-β-gal were observed at 20 Gy, where most cells of all species showed positive staining. *E. spelaea* was an exception, as it did not show positive SA-β-gal staining at pH-6.0 and therefore could not be quantified (Fig. 3b). This could be because of species-specific differences in SA-β-gal. However, these fibroblasts showed a flat and enlarged appearance typical of senescent cells. In summary, some bat fibroblasts displayed attenuated levels of SIPS compared to mouse and human cells.

Senescent cells are characterized by the release of autocrine and paracrine secretory factors known as Senescence Associated Secretory Proteins (SASP)[42,43]. Transcriptomes from fibroblasts treated with γ-radiation and allowed to senesce for 12 d were analyzed for SASP factors and other signatures of senescence. Gene Set Enrichment Analysis

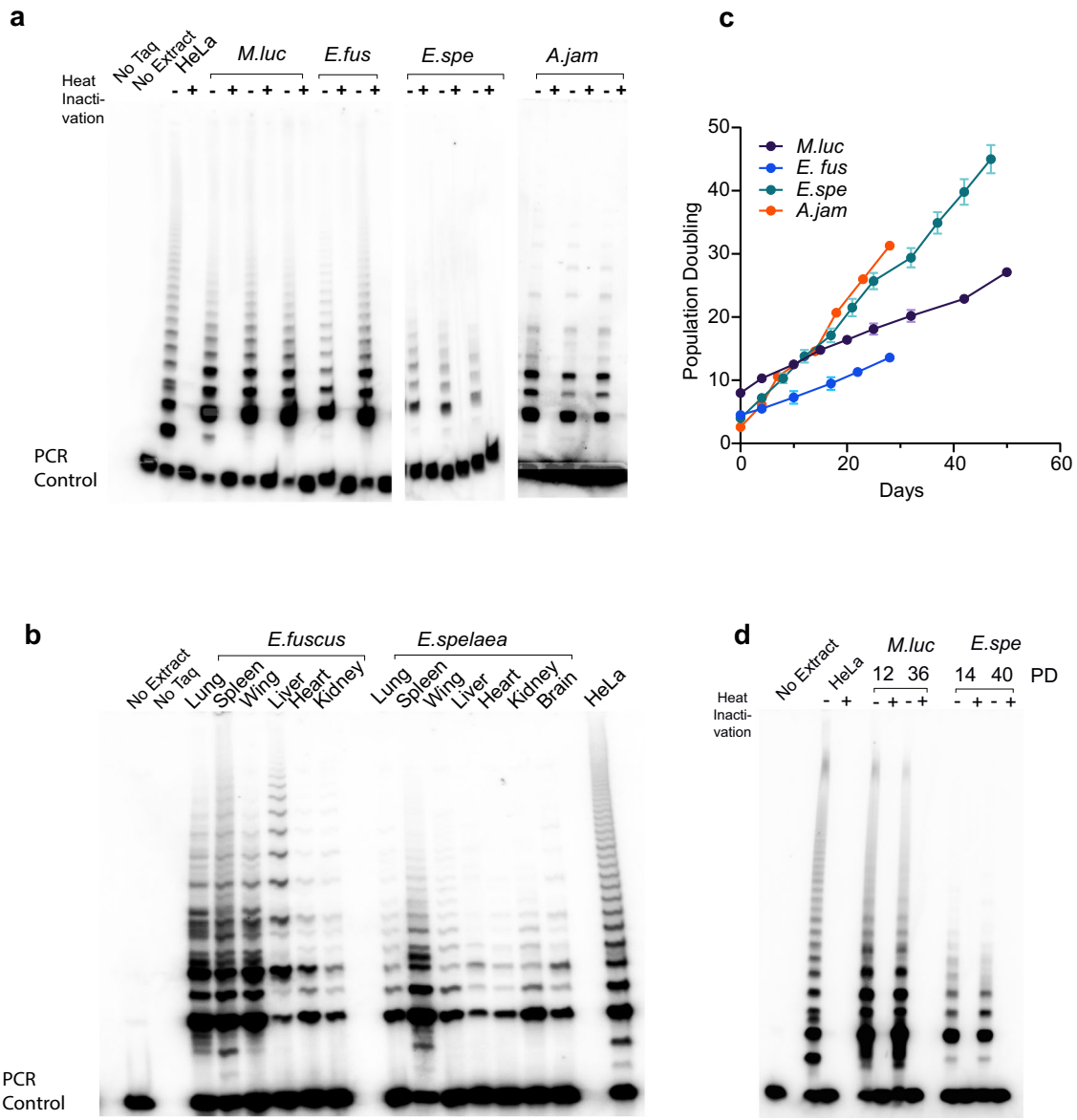

Fig. 1 | Bat cells and tissues possess telomerase activity. Telomerase Repeated Amplification Protocol (TRAP) assay is shown using wing fibroblasts or tissue extracts from bat species listed- *M. lucifugus* (*M.luc*), *E. fuscus* (*E.fus*), *E. spelaea* (*E.spe*) and *A. jamaicensis* (*A.jam*). HeLa extract was used as the positive control, and the heat-inactivated extract of each sample was used as a negative control. Internal PCR control is used to show the absence of PCR inhibitors in samples. **a** Telomerase activity in bat wing fibroblasts derived from four different species. Experiments were repeated with $n = 3$ individual bats/species with similar results. **b** Representative TRAP assay showing telomerase activity in several tissues of bats *E. fuscus* and *E. spelaea*. Experiments were repeated with $n = 2$ individual bats/species with similar results. **c** Population doubling curves for four species of bats showing fibroblast growth rates in culture. Data are presented as mean ± SD. *M. luc*, $n = 2$; *E. fus*, $n = 3$; *E. spe*, $n = 2$; *A.jam*, $n = 3$ individual bats. **d** Representative TRAP assay showing telomerase activity in bat wing fibroblasts of *M. lucifugus* and *E. spelaea* differing by at least 20 population doublings. Experiments were repeated with $n = 2$ individual bats/species with similar results. Source data are provided as a Source Data file.

https://doi.org/10.1038/s41467-025-59403-z

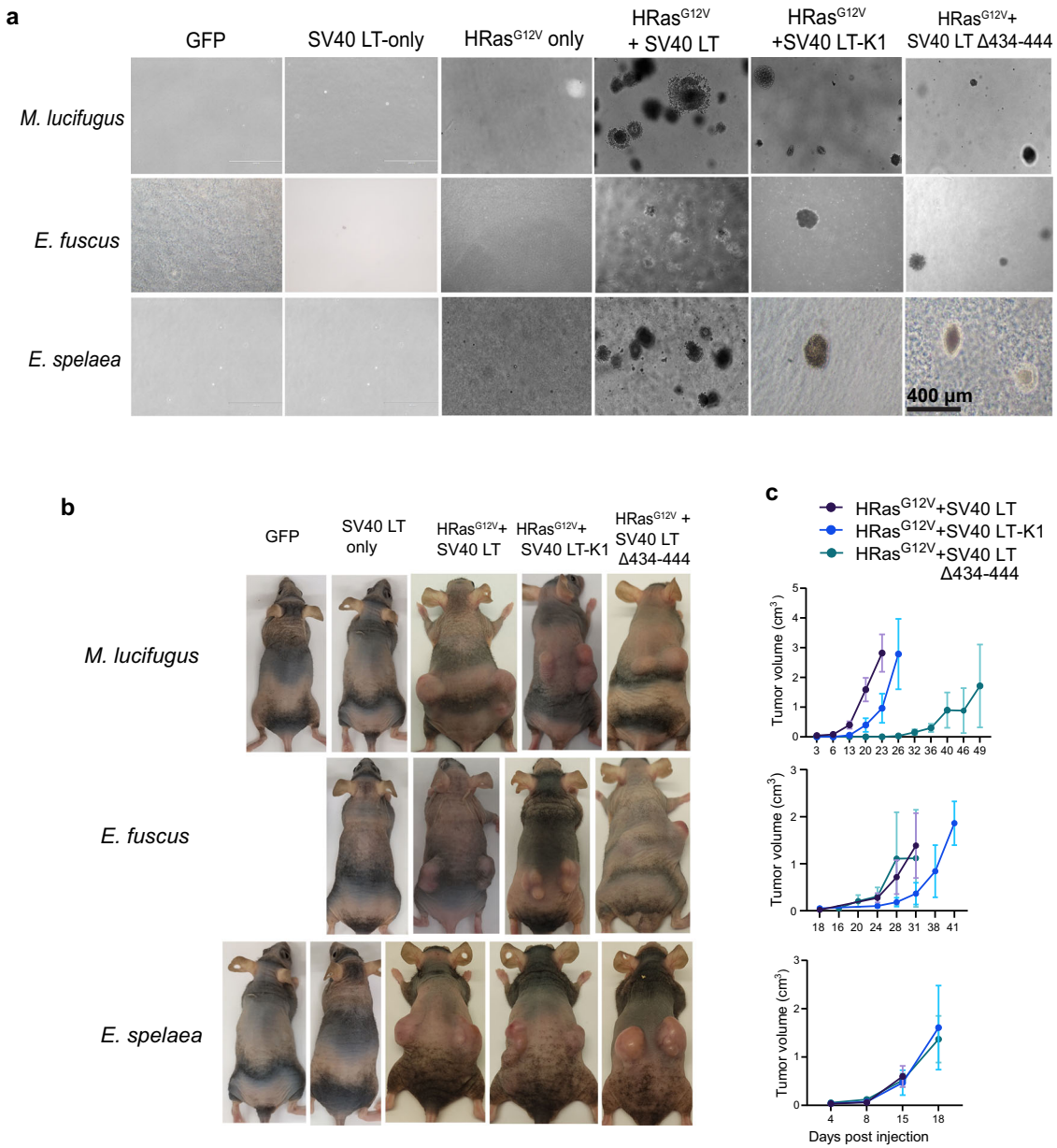

Fig. 2 | Two oncogenic hits are sufficient for transformation of bat fibroblasts. **a** Representative images of colonies formed in soft agar assay by transformed bat wing fibroblasts from 3 bat species, *M. lucifugus* ($n = 3$), *E. fuscus* ($n = 2$), and *E. spelaea* ($n = 3$), at the end of three weeks. n= individual bats. Scale bar, 400 μm. Overexpression of HRas^{G12V} along with SV40 LT constitutes 3 oncogenic hits, while HRas^{G12V} along with either mutant of SV40 LT constitutes 2 oncogenic hits. **b** Mouse xenograft assay using bat wing fibroblasts overexpressing oncogenes form tumors in nude mice. Transformed cell lines from one individual bat per species was tested in the xenograft assay. Each cell line was tested with 8 injections in nude mice. Images shown were taken at the experiment endpoint. **c** Tumor growth curves of transformed bat wing fibroblasts show increase in tumor volumes with time in mouse xenograft assay. Tumor volumes are shown as mean ± SD, $n = 8$ injections/cell line. Error bars show standard deviation (SD). Source data are provided as a Source Data file.

(GSEA) was performed using SASP gene sets from published literature[44–46]. At 10 Gy, *M. lucifugus* showed downregulation of several SASP factors that are generally upregulated during senescence (Fig. 4a). This was also reflected in SA-β galactosidase staining, where *M. lucifugus* showed a lower percentage of senescent cells at 10 Gy. Detailed analysis of SASP gene expression showed that senescent *M. lucifugus* cells at lower doses of radiation altered expression of only about 30% of SASP genes compared to about 70% altered in mouse (Fig. 4b). *E. fuscus*, *E. spelaea*, and *A. jamaicensis* also showed a lower fraction of genes upregulated in some SASP categories when compared to mice in a similar analysis (Supplementary Fig. 2). Because interferons are one of the components of SASP, we directly compared interferon expression in radiation-treated cells from two different time points, 24 h and 12 days post-radiation. Analysis of interferon expression revealed that senescent bat fibroblasts showed remarkably low interferon responses compared to human and mouse fibroblasts (Fig. 4c).

Bat cells display elevated p53 activity

Genomic instability caused by γ-radiation treatment may lead to apoptosis. Apoptosis assays on day 3 post-radiation showed that most species of bats displayed significant increase in apoptosis upon irradiation with 10 and 20 Gy doses, in contrast to mice and human cells (Fig. 5a). Elevated apoptosis in bats was also observed with lower doses of γ-radiation (2 and 6 Gy) (Supplementary Fig. 1f). Since we observed elevated apoptosis in bat cells following γ-radiation we hypothesized

https://doi.org/10.1038/s41467-025-59403-z

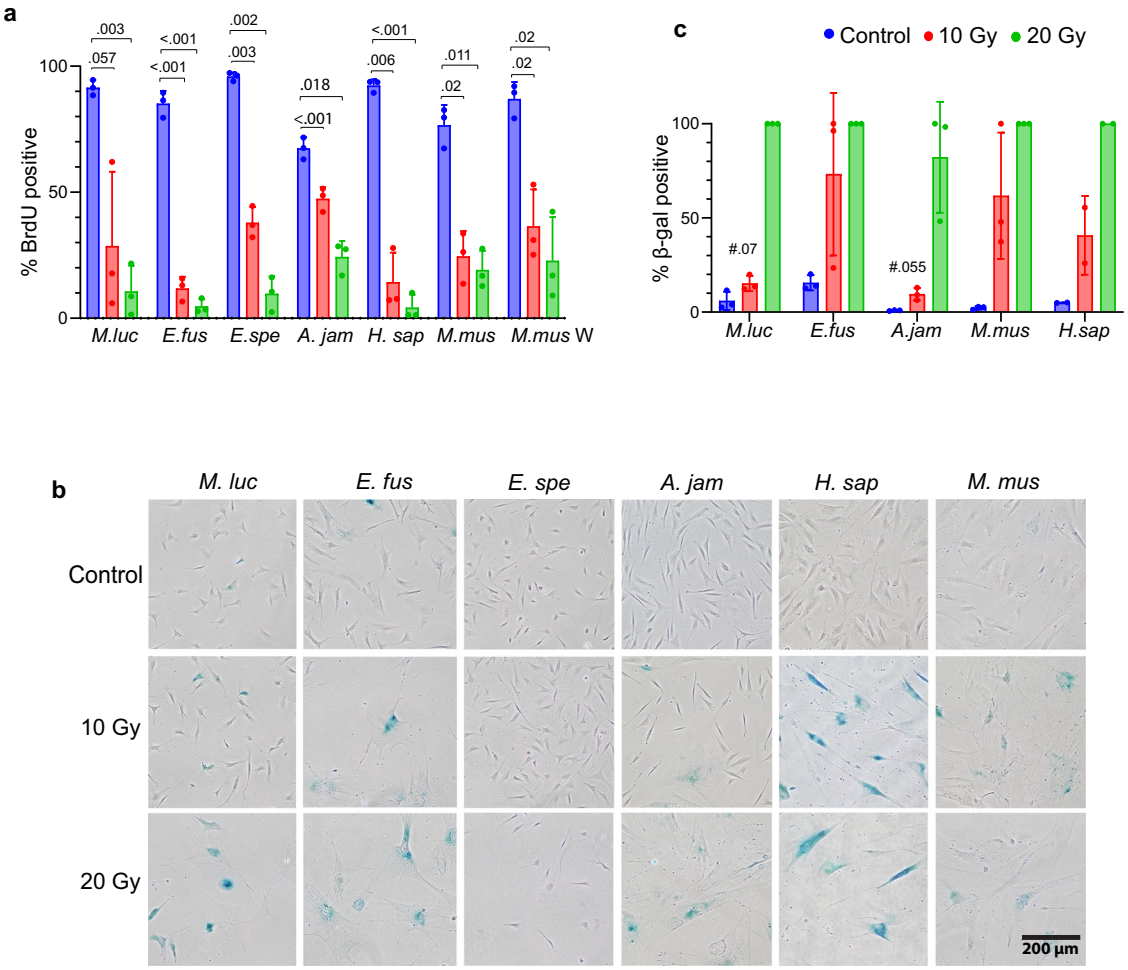

Fig. 3 | Analysis of senescence in bat species day 12 post-radiation. a BrdU incorporation assay, day 3 post-radiation in bat wing fibroblasts. $n = 3$ biological replicates, data are presented as mean ± SD. Comparison to intra-species controls was done using a paired two-tailed t test. Interspecies comparisons, between bats and wild-caught mice, for similar conditions were made using unpaired two-tailed t tests and are indicated with symbol '#'. **b** Representative SA-β gal staining images of fibroblasts from all species 12 days post-radiation treatment. $n = 3$ biological replicates. Scale, 200 µm. **c** Quantification of SA-β gal staining showing percentage of positively stained cells. Data are presented as mean ± SD, $n = 3$ biological replicates. Comparison to intra-species controls was done using a paired two-tailed t test. Interspecies comparisons, between bats and laboratory mice, for similar conditions was done using unpaired two-tailed t tests and is indicated with the symbol '#'. P-values are indicated. Source data are provided as a Source Data file.

that bats may display elevated p53 activity. We tested p53 reporter activity in untreated fibroblasts from all species. We found that basal p53 transcriptional activity was higher in bat fibroblasts when compared to humans and mice. The vespertilionid bats, *M. lucifugus* and *E. fuscus,* showed at least four-fold higher p53-reporter activity, while *E. spelaea* and *A. jamaicensis* showed about 1.5-2-fold higher activity compared to humans and mice (Fig. 5b). Cells transfected with SV40 LT-K1 mutant, which specifically inhibits p53 function, demonstrated the specificity of the reporter activity. We then treated cells with Nutlin-3, an Mdm2 agonist, which stabilizes p53 by inhibiting Mdm2-mediated p53 degradation. Bat fibroblasts showed higher apoptosis than mouse and human fibroblasts following treatment with Nutlin-3 (Fig. 5c).

We performed RNA sequencing of bat wing fibroblasts from *M. lucifugus*, *E. fuscus*, *E. spelaea*, and *A. jamaicensis,* along with skin fibroblasts from laboratory mice, wild-caught *Mus musculus* mice, and humans treated with 10 and 20 Gy doses of γ-radiation, at two time points, 24 h and 12 days post-radiation treatment. Both principal component analysis (PCA) and hierarchical clustering showed species-wise clustering of samples (Supplementary Figs. 1a, b). Transcript levels of p53 were elevated in untreated bat fibroblasts compared to human skin fibroblasts (Fig. 6a, b). The transcript profile of *TP53* in skin fibroblasts from mice was comparable to that of bats, although they did not show higher transcriptional activity in the functional reporter assay in cells.

We then analyzed *TP53* transcriptional targets and regulators (Fig. 6e). *M. lucifugus*, *E. fuscus*, and *A. jamaicensis* showed upregulation of *BAX*, a direct transcriptional target involved in p53-mediated apoptosis, along with *BCL2*[47]. *MDM2* (mouse double min 2) is a key p53 antagonist that regulates p53 in a ubiquitination-dependent and independent manner[48,49]. *MDM2* transcripts were upregulated in *M. lucifugus* and *E. fuscus* (Fig. 6c). *WRAP53* (WD40 encoding RNA anti-sense to *TP53*) is a natural anti-sense transcript nested in the *TP53* gene[50,51]. All bats showed higher levels of *WRAP53* transcripts when compared to humans and mice, in both treated and untreated cells. *A. jamaicensis* showed higher levels of *WRAP53* transcripts compared to other bat species (Fig. 6d).

DNA repair genes have been shown to be positively selected in bats[25,52]. Genes involved in DNA damage *(ATM, ATR, ChEK1, GADD45A, PCNA*) and cell cycle arrest genes (*CDKN1A, CCNG1*) were upregulated in most bat species (Fig. 6e). *PCNA* showed higher upregulation in *M. lucifugus* in radiation-treated cells. Basal levels of Cold-induced RNA binding protein (*CIRBP*) with roles in DNA double-strand repair and stabilization of transcripts involved in cellular stress levels were higher

https://doi.org/10.1038/s41467-025-59403-z

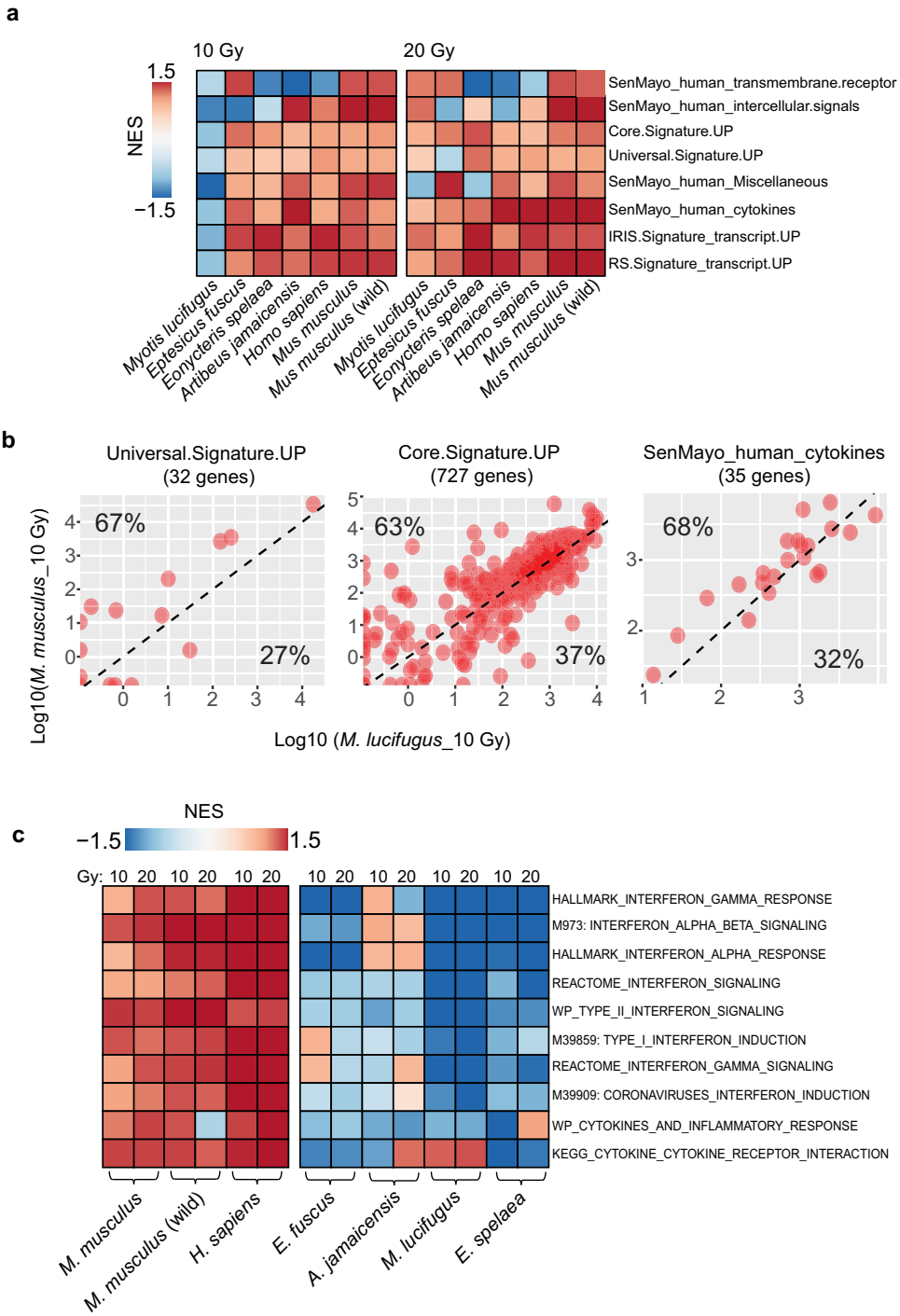

Fig. 4 | Comparative analysis of SASP in transcriptome of senescent fibroblast from bats, humans, and mice. a Gene Set Enrichment Analysis (GSEA) of transcriptome using senescence-related gene sets, day 12 post-radiation. Gene sets were collected from the MsigDB database and published literature (See "Methods"). **b** Scatter plots showing the expression differences between *M. lucifugus* and mouse senescent fibroblasts day 12 post-radiation in 3 SASP-related gene sets. Percentages in the left-upper and lower-right in the plot indicate the fraction of genes with higher expression in mouse and *M. lucifugus*, respectively. **c** GSEA analysis of inflammation-related gene sets in senescent fibroblasts, day 12 post-radiation. For this analysis, radiation-treated cells from 12 days were compared to those from 24 h post-radiation. Source data are provided as a Source Data file.

in *E. fuscus, E. spelaea*, and *A. jamaicensis* compared to humans and mice[53] (Fig. 6e).

We further performed GSEA using different p53 pathway gene sets. Since p53 is the universal pathway activated on radiation treatment, all species showed enrichment of p53 pathway terms (Fig. 6f). However, *M. lucifugus* showed higher enrichment for some of the *TP53*-related pathway terms compared to other species. For example, genes of Reactome terms like "Transcription of cell cycle genes, G2, G1- cell cycle arrest", "Regulation of *TP53* activity by phosphorylation" were upregulated in *M. lucifugus*. The proapoptotic term "Reactome *TP53* regulates transcription of genes involved in cytochrome C release" was also highly enriched in *M. lucifugus* at 10 Gy (Fig. 6f).

GSEA for different pathways involved in DNA repair showed that *M. lucifugus* cells treated with 20 Gy showed slightly higher enrichment

https://doi.org/10.1038/s41467-025-59403-z

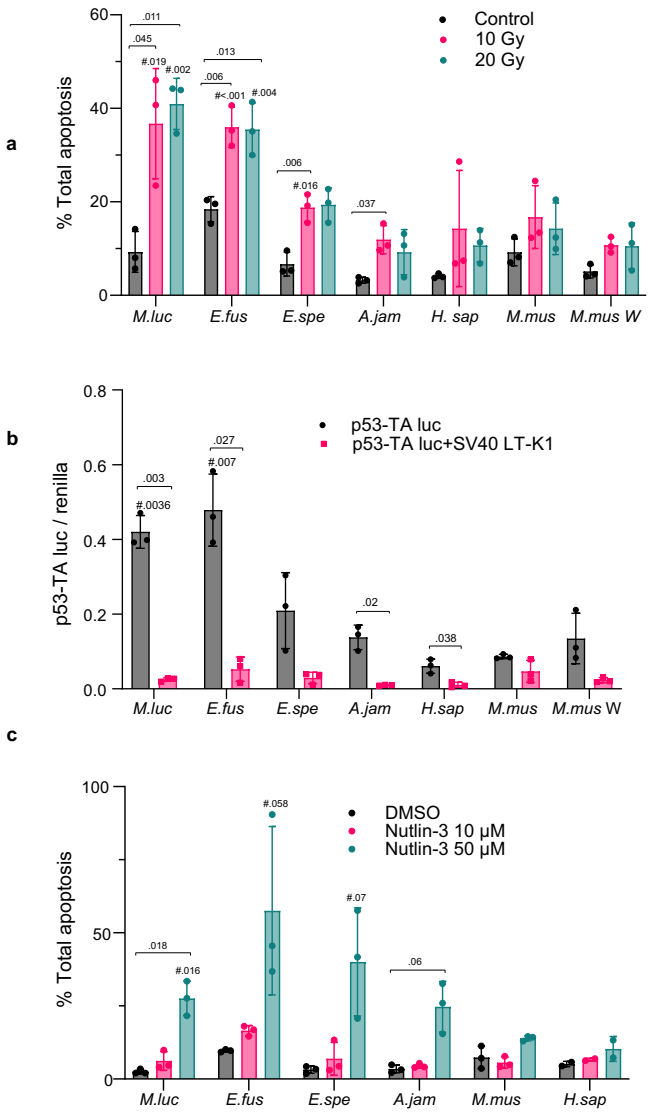

Fig. 5 | Bat fibroblasts undergo higher TP53-mediated apoptosis on treatment with γ-radiation. a Annexin V apoptosis assay in bat fibroblasts treated with 10 and 20 Gy γ-radiation, day 3 post-radiation treatment. Interspecies comparisons, between bats and wild-caught mouse, for similar conditions were made using unpaired two-tailed *t*-tests and are indicated with the symbol '#'. **b** p53-TA-luciferase reporter activity in normal proliferating bat wing fibroblasts and skin fibroblasts from mice and humans. Interspecies comparisons, between bats and wild-caught mouse, for similar conditions were made using unpaired two-tailed *t* tests and are indicated with the symbol '#'. **c** Annexin V apoptosis assay in proliferating cells treated with Nutlin-3 for 6 h. Interspecies comparisons, between bats and laboratory mouse, for similar conditions were made using unpaired two-tailed *t* tests and are indicated with the symbol '#'. Data are presented as mean ± SD. $n = 3$, biological replicates. Comparison to intra-species controls was done using a paired two-tailed *t*-test. All *p*-values are indicated. Source data are provided as a Source Data file.

for DNA repair pathway terms at 24 h post-radiation treatment (Fig. 6f). However, overall, the DNA repair pathway terms were not specifically enriched in all bat species in our data sets.

Multiple copies of *TP53* in *Myotis lucifugus*

A p53-mediated apoptotic response to SIPS was also observed in a previous study with elephant fibroblasts. It was shown that the expansion of *TP53* copy number in elephants (20 copies) with several *TP53* retrogenes showing expression could be responsible for this phenotype[17,18,54]. We analyzed genomes of several bat species to see if *TP53* copy number expansion has occurred in Chiroptera (Fig. 7a). We found that several bat species have 2–4 copies of *TP53*. Most intriguingly, the vespertilionid bats in this study, *M. lucifugus* and *E. fuscus*, seem to possess 7 and 3 copies of *TP53*, respectively. Of the seven copies of *TP53* in *M. lucifugus*, one full copy duplication and five short retrocopies seem to exist in the available genome assembly, Myoluc2.0 (GCA_000147115.1). Potentially erroneous copy number estimation can result from a fragmented genome assembly. Therefore, we further analyzed and found the two copies in the HiC-guided assembly of the *M. lucifugus* genome (Myoluc2.0_HiC)[55,56]. We additionally performed Cas9-targeted sequencing using guides directed to *TP53* copies in the *M. lucifugus* genome and obtained one long read (118 K) covering the *TP53* region of *M. lucifugus* in our preliminary analysis. This long read sequence suggests the presence of two full-length copies of *TP53* (Fig. 7b).

Discussion

Bats are very long-lived for their size, and tumors are rarely found in bats[6,10–13]. The number of oncogenic hits required for malignant transformation highlights species-specific inherent barriers to cancer development. For example, human fibroblasts have been shown to require five oncogenic hits for transformation (activation of telomerase, oncogenic Ras signaling, inactivation of p53, pRb, and PP2A), whereas mice require only two (inactivation of either pRb or p53 and activation of Ras signaling)[38]. The number of oncogenic hits generally increases with body size and lifespan. For example, chinchilla and porcupine fibroblasts require 3 hits, naked mole rat fibroblasts require 4 hits, and beaver fibroblasts require 5 hits[15]. Here we discovered, unexpectedly, that all three species of bats tested, *M. lucifugus*, *E. fuscus*, and *E. spelaea*, representing the two bat suborders, underwent malignant transformation with two hits - the expression of $HRas^{G12V}$ and inactivation of either pRb or p53. This suggested that bat fibroblasts are easily transformed and do not possess any peculiar inherent barriers to cell transformation. We also tested if our observation holds true in bat epithelial cells and if they can be easily transformed. We were able to derive kidney epithelial cells from *E. fuscus* and tested their ability to undergo oncogenic transformation using $HRas^{G12V}$ and SV40 LT. Like their corresponding fibroblasts, kidney epithelial cells from *E. fuscus* were easily transformed and were capable of adherence-independent growth in soft agar assay (Supplementary Fig. 1h). While we were drafting this manuscript, a similar study was published reporting that fibroblasts from seven different bat species, native to the Asian continent, undergo malignant transformation with overexpression of $HRas^{G12V}$ and SV40 LT antigen[37], indicating that this ease of malignant transformation is a wide spread phenomenon in bats. Transformed colonies of one of the seven bat species, *Myotis pilosus*, a member of the longest-lived genera of bats, proliferated more slowly, which led the authors to identify a decrease in expression of *HIF5*, *COPS5*, and *RPS3* as potential mechanisms of cancer resistance in this particular bat[37]. However, this does not explain the paradox why species whose cells can be transformed with only two oncogenic hits show cancer resistance in vivo.

Downregulation of somatic telomerase activity is a tumor suppressor mechanism that evolved in mammals with a body mass larger than 5–10 kg[40]. Cancerous cells in these species must re-activate telomerase or use alternate telomerase pathways for survival[15,57]. The presence or absence of telomerase activity in somatic cells and tissues has been tested only for a few bat species[16]. It has been observed that transcript levels of *TERT* are generally low in somatic cells, and PCR-based enzymatic assays are a better readout for telomerase activity. Having tested five bat species representing different clades, using the TRAP assay, we confirm that bats have telomerase activity in their somatic cells and tissues, which is consistent with their body mass being below 5 kg. Within the five bat species that we tested, smaller bats *M. lucifugus, Myotis myotis*, and *E. fuscus* (body weight 5–40 g)

https://doi.org/10.1038/s41467-025-59403-z

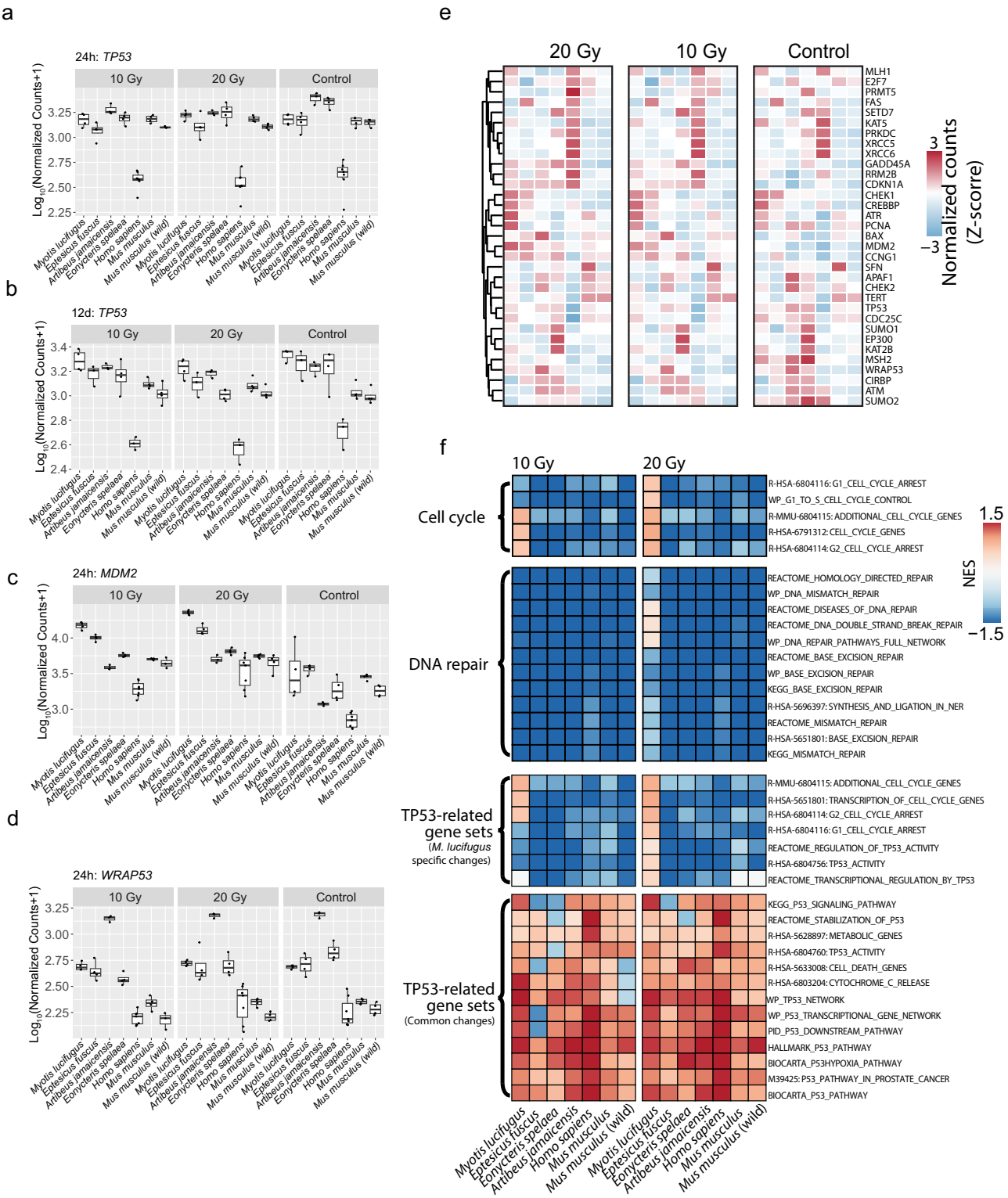

Fig. 6 | Functional enrichment analysis of TP53-related gene sets after irradiation. a, **b** Boxplots showing *TP53* transcript levels in untreated control and radiation-treated cells at (**a**) 24 h and (**b**) 12 days post-radiation. The box plots display the median, the 1st, and 3rd quartiles; the whiskers show a 1.5 × interquartile range. Data points outside the whiskers are outliers. **c**, **d** Boxplots showing the expression changes of (**c**) *MDM2* and (**d**) *WRAP53* in each species at 24 h post-radiation. The box plots display the median, 1st, and 3rd quartiles; the whiskers show a 1.5 × interquartile range. Data points outside the whiskers are outliers. *M. lucifugus* $n = 4$ ($n = 3$ in 12 d control); *E. fuscus* $n = 4$ ($n = 3$ in all 12 d samples); *A. jamaicensis* $n = 4$ ($n = 3$ in all 12 d samples); *E. spelaea* $n = 4$; *H. sapiens* $n = 7$ ($n = 3$ in all 12 d samples); *M. musculus* (wild) $n = 4$ ($n = 3$ in 24 h:10 Gy). **e** Heatmap showing the expression changes of *TP53* related genes 24 h after irradiation. **f** GSEA analysis for cell cycle, DNA repair, and *TP53* related gene sets in fibroblasts 24 h post-radiation. Source data are provided as a Source Data file.

https://doi.org/10.1038/s41467-025-59403-z

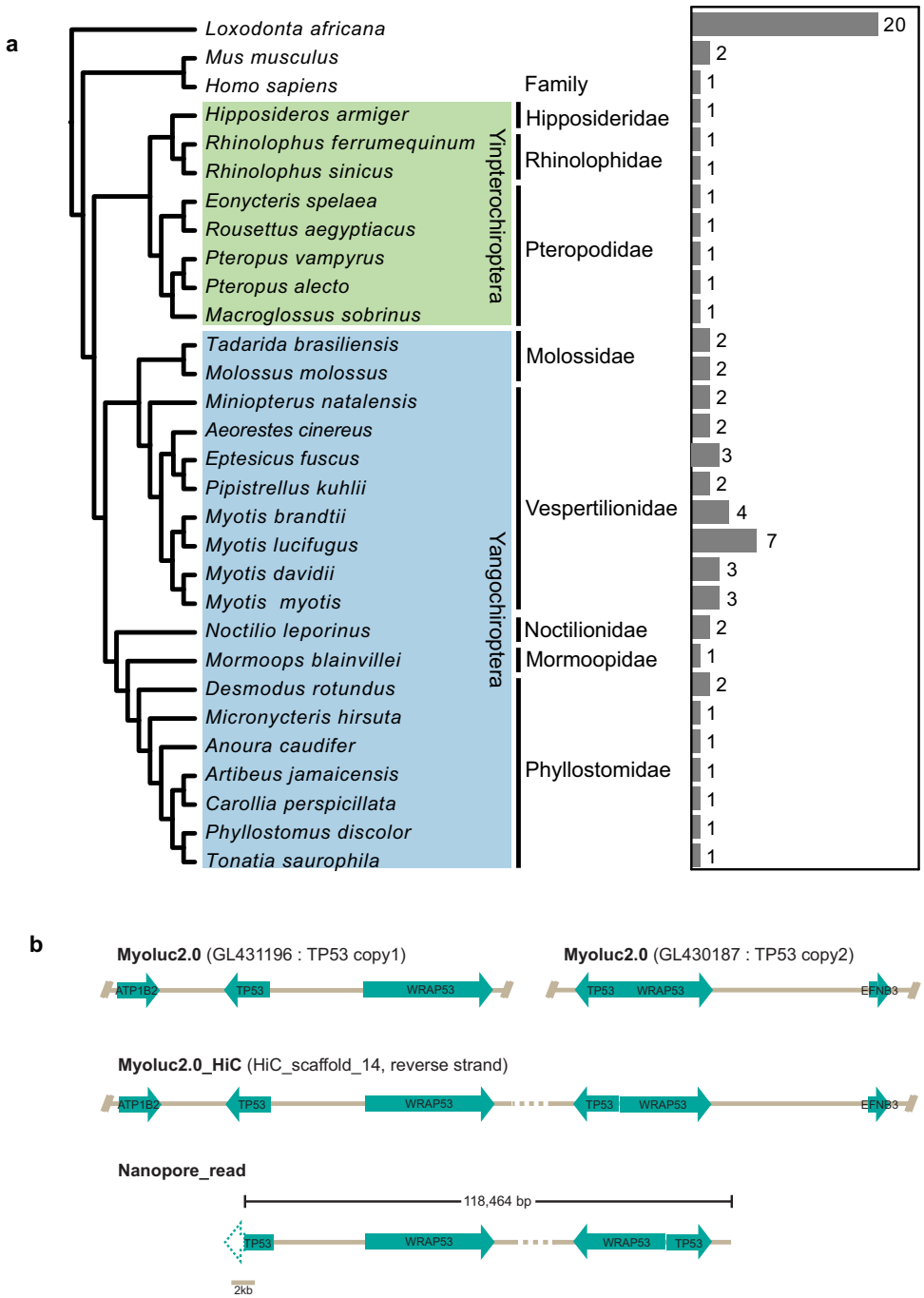

Fig. 7 | Analysis of *TP53* copy numbers in bats. a *TP53* copy numbers are shown as the bar at the right side. The phylogenetic relationship between species were collected from https://vertlife.org/. **b** *TP53* full copy duplications from genome, HiC-guided assembly, and long-read sequencing in *M. lucifugus*.

showed higher telomerase activity than larger bats, *E. spelaea*, and *A. jamaicensis* (40–80 g). This fit the general negative correlation between somatic telomerase activity and body mass, independent of lifespan[40].

Although bat cells expressed telomerase and did not experience replicative senescence, they could be induced to undergo SIPS using γ-radiation. Senescence is characterized by irreversible cell cycle arrest and release of pro-inflammatory factors called senescence-associated secretory phenotype (SASP) by the senescent cells[42,43,58]. The senescence program is a double-edged sword, though it prevents the inheritance of mutations precluding potential malignant transformation, it also promotes age-related inflammation contributing to the aging process[59]. *M. lucifugus* showed distinct features in our analysis of SASP in senescent bat fibroblasts. Senescent *M. lucifugus* cells showed a markedly low SASP factor expression, suggesting that this bat may avoid the negative aspects of senescence. All bat species exhibited a blunted inflammatory response, with significantly lower interferon expression than non-bat species (Fig. 4c). Bats show reduced pro-inflammatory responses, contraction of the type I interferon family and constitutive expression of interferon-α genes in cells and tissues, loss of PYHIN locus, and dampened activation of NLRP3 inflammasome[25,34,60,61]. These unusual immune adaptations in bats, which may have evolved to counteract damage due to increased metabolism and higher body temperatures during flight, or for the co-existence with viruses, may have been co-opted against the inflammation induced by senescent cells.

We observed that bat fibroblasts, when exposed to genotoxic stress, displayed enhanced apoptosis when compared to mice and humans. p53 is the primary responder to genotoxic stress and can induce apoptosis on extensive DNA damage[62]. We found that bat fibroblasts have enhanced basal *TP53* transcript levels. All four species had higher levels of *TP53* transcripts and showed two to four times higher basal transcriptional activity than in human or mouse cells. Higher transcript levels were sustained in cells upon radiation treatment and induction of senescence. Direct transcriptional targets of *TP53,* like *CDKN1A*, *CCNG1* (cell cycle arrest), *MDM2* (p53 regulator), and *BAX* (proapoptotic factor)[63], were upregulated in most species, albeit with enhanced levels in some bats. Since skin tissue predominantly consists of epithelial cells, we analyzed *TP53* transcript expression in the skin tissue transcriptome of three bats species. When compared to mouse skin, we found that *TP53* transcript levels were higher in bats (Supplementary Fig. 2c). We speculated if higher *TP53* transcription levels could be caused by transposons inserting nearby and providing promoter on enhancer sequences. Indeed, we found that in both bats and non-bat species, the 20 Kb upstream sequences of the 1st coding exon of *TP53* are enriched in TEs, especially in the 3rd intron of *WRAP53,* which partially overlaps with the *TP53*. These 20 Kb upstream sequences are predicted to contain many high-confidence promoters in all species examined (Supplementary Fig. 2d), which may include original and TE-derived promoters. Interestingly, we found that bats without *TP53* duplication have higher number of predicted promoters (6–7 predicted promoters) compared to mice, human, and other mammals (5 predicted promoters) (Supplementary Fig. 2d). Therefore, in these bat species, these extra promoters can potentially enhance *TP53* transcript levels even without gene duplications.

How do bat cells tolerate higher p53 protein levels in their cells? Our transcriptome analysis provides few clues, although no universal pattern applicable for all four bat species emerges. Bat fibroblasts treated with radiation upregulated *MDM2*, with most upregulation seen in the vespertilionid bats *M. lucifugus* and *E. fuscus* (Fig. 6c). *MDM2*, a transcriptional target of *TP53*, is an E3 ubiquitin ligase that negatively regulates TP53 activity by ubiquitin-dependent and independent mechanisms[48,49]. Interestingly, bat-specific nucleotide changes in the nuclear localization signal of *TP53* and nuclear export signal of *MDM2* are reported, which may alter the pattern of transactivation by changing some of the numerous sites on p53 that undergo posttranslational modifications, providing a fine tuning of p53 activity in response to various stimuli[25]. *WRAP53* is a natural antisense transcript of *TP53* and, in a non-reciprocal manner, positively regulates p53 activity by preventing degradation of *TP53* mRNA[50,51]. All four bat species show enhanced basal levels of *WRAP53*, sustained following radiation treatment, and not observed in humans or mice. *A. jamaicensis* shows the highest expression of *WRAP53* expression (Fig. 6d). Additionally, p53 was shown to undergo positive selection in *M. davidi, one of the longest-lived bats*[25]. Interestingly, *FBXO31,* which promotes degradation of Mdm2 to increase p53 levels[64], underwent massive expansion in microbats with *Myotis lucifugus* and *Myotis brandtii* genomes containing over 50 copies[33,36,65]. This expansion may also increase p53 levels and activity.

Enhanced reliance on apoptosis has been observed in the other long-lived and cancer-resistant species, the elephants. It was shown that the expansion of *TP53* copy number in elephants (20 copies) with several *TP53* retrogenes showing expression could be responsible for this phenotype[17,18,54]. We analyzed genomes of several bat species to see if *TP53* copy number expansion has occurred in Chiroptera. We found that several microbats have 2–4 copies of *TP53*. Most intriguingly, the vespertilionids in this study, *M. lucifugus* and *E. fuscus*, seem to possess 7 and 3 copies of *TP53*, respectively. Of the seven copies of *TP53* in *M. lucifugus*, one is a full copy duplication and five are short retrocopies. Whether the p53 duplication plays a role in enhanced basal p53 levels remains to be determined. Elevated p53 activity is likely to contribute to cancer resistance in bats, as increasing p53 dosage in mice significantly increased their resistance to cancer[66,67].

Overall, bats have been shown to have several pro-tumorigenic characteristics such as flight-related high metabolism and oxidative stress, DNA damage, viruses[34,68–70], and from this study, lack of replicative senescence, easy oncogenic transformation of cells, and sustained telomerase activity. However, these may be counterbalanced by adaptations that lower oxidative stress, torpor-related lower metabolism, adaptations in GH/IGF1 axis, enhanced DNA repair[25,34,36,71–73], and from our study, anti-tumorigenic properties like apoptotic response to genotoxic stress, lower SASP and inflammatory response to radiation stress, and enhanced expression of tumor suppressor protein, p53. Furthermore, bats have unique immune systems which allows them to survive a wide range of deadly viruses, and many unique immune adaptations have been described in bats (reviewed in ref. 34). Most knowledge of the bat immune systems comes from studies of bat tolerance to viral infections deadly to humans. However, these or similar immune adaptations may also recognize and eliminate tumors. No direct experimental evidence of immune surveillance or cancer immunoediting is available in bats. Chronic inflammation is known to facilitate tumor formation[74], and the common immune adaptation found in bats is reduced inflammation when exposed to pathogens. CD8 + T cells, Natural Killer (NK) cells, and macrophages have roles in the immune surveillance of tissues. Single-cell and genomics analysis have shown an expanded and diverse KLRC/KLRD family of natural killer cell receptors, MHC class I genes, and type I interferons in *Rousettus aegyptiacus*[27]. *R. aegyptiacus* also showed novel subsets of monocytes in response to pathogenic stimuli and unique leukocyte transcriptional subsets in circulation[75,76]. A high proportion of CD8 + T cells, tissue-resident memory T cells, and long-lived effector memory natural killer T-like cells were shown to occur across 19 organs in *Rhinolophus sinicus*[77]. More interestingly, an analysis of juvenile and adult *Rousettus aegyptiacus* revealed an unchanged lymphocyte proliferative capacity with age[76].

The NK cells have been shown to be a critical cell type mediating immune surveillance of tumor cells. We analyzed bulk RNA-seq data from tissues of big brown bat (*E. fuscus*), cave nectar bat (*E. spelaea*), Jamaican fruit bat (*A. jamaicensis*) and rat, mouse, and naked mole rats[78] and compared them to the NK cell-related transcriptome signatures from published studies[79–81] and MsigDB (Supplementary Fig. 1g). Remarkably, all the comparisons show higher expression of the 3 NK signatures in bats, indicating that the NK cell composition in bat skin is higher compared to non-bat species. Although awaiting direct experimental evidence, these studies suggest that bats may rely on enhanced immune surveillance to eliminate pre-malignant cells from their tissues.

In summary, our study demonstrates that bat fibroblasts undergo malignant transformation with just two oncogenic hits. Bat cells constitutively express telomerase and do not need to bypass the replicative senescence barrier for malignant transformation. We also show that bats have elevated transcriptional levels and signaling through p53 pathways with some species showing genomic duplications (Fig. 8). Given the current knowledge of the unique immune adaptations in bats, we hypothesize, that bats may rely more on non-cell autonomous tumor suppressor mechanisms for elimination and detection of cancerous cells in vivo.

Limitations of the study: Fibroblasts have been traditionally used for cross-species studies of malignant transformation, as other cell types require unique culture conditions that, in many cases, are species-specific and have not been established for the exotic species. However, requirements for malignant transformation may differ across cell types. Therefore, the conclusions of this study are limited to fibroblasts.

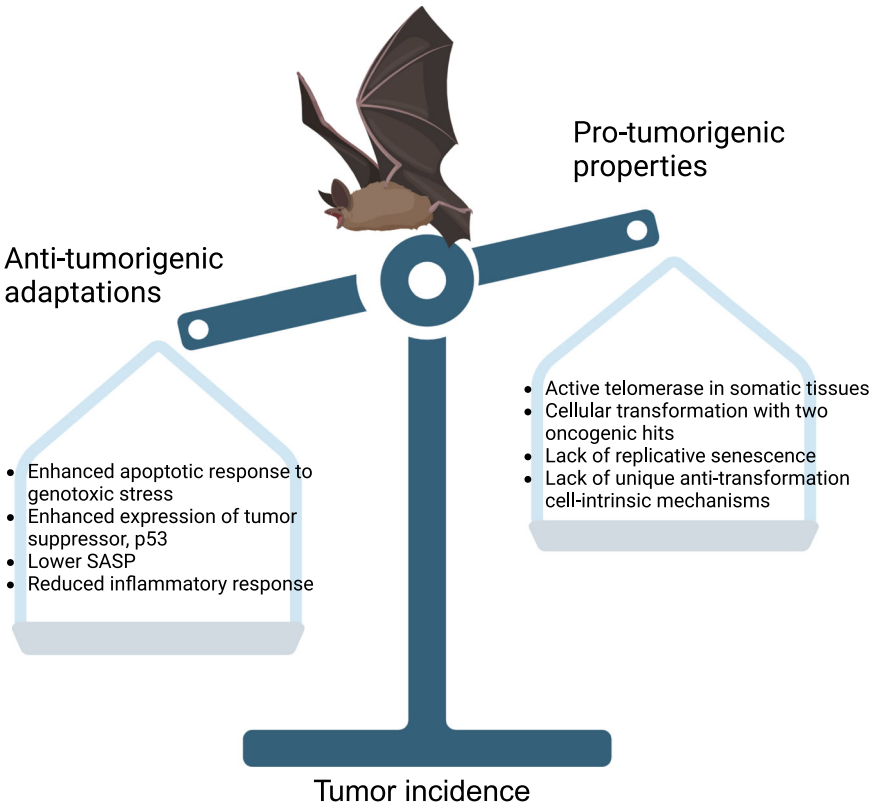

Fig. 8 | Graphical summary. Our findings suggest that bat fibroblasts possess pro-tumorigenic characteristics like a lack of replicative senescence, easy oncogenic transformation, and sustained telomerase activity, and are easily transformed with two oncogenic hits. However, they also possess anti-tumorigenic properties like apoptotic response to genotoxic stress, lower SASP, and enhanced expression of tumor suppressor protein, p53. We hypothesize that a balance of these properties and non-cell autonomous factors, like their unique immune system adaptations, may contribute to their resistance to cancer. Created in BioRender. Athar, F. (2025) https://BioRender.com/b33q059.

Methods

Animals

All animal experiments were approved by the University of Rochester Committee for Animal Research (UCAR), Protocol number 2017-033, and complied with relevant ethical regulations. *Myotis lucifugus* wing fibroblasts from three individuals were from Richard Miller collection at the University of Michigan. *Eptesicus fuscus* fibroblasts were isolated from wing tissue of four individual bats from the Northeast Ohio Medical University colony. *Eonycteris spelaea* fibroblasts were isolated from wing tissue of four individual bats from a breeding colony housed at Duke NUS in Singapore. *Artibeus jamaicensis* fibroblasts were isolated from wing tissue of four individual bats from the Colorado State University colony. Maximum lifespan (MLS) information for *M. lucifugus*, *E. fuscus*, and *A. jamaicensis* were obtained from AnAge[82]. MLS for *E. spelaea* is from personal communication from bat researchers. *Myotis myotis* were sampled in Morbihan, Brittany in North-West France, July 2021 in accordance with the permits and ethical guidelines issued by 'Arrête´' by the Préfet du Morbihan (Brittany) and the University College Dublin ethics committee. This population has been transponded and followed since 2010 as part of on-going mark-recapture studies by Bretagne Vivante and the Teeling laboratory.

Cell culture

Primary fibroblasts were isolated from wing tissue of big brown bats, cave nectar bats, and Jamaican fruit bats, and little brown bats using a published protocol[83]. Briefly, about 1 cm2 wing tissue was minced ~1 mm pieces using a scalpel. Minced tissue was digested for 30–45 min in 10 ml of DMEM/F12 (Fisher Scientific, 11-320-082) media with Liberase™ (Millipore Sigma, 5401127001) and 1X antibiotic/antimycotic (Sigma-Aldrich, 15240062) at 37 °C. The digested tissue was washed 3X with DMEM/F12 containing 15% FBS, 1X antibiotic/antimycotic. The digested tissue pellet was resuspended and plated in the same media and allowed to grow for 3–7 days with media replenishment as required[83]. Isolated wing fibroblasts were then grown in EMEM (ATCC) containing 15% fetal bovine serum (GIBCO), 100 U/mL penicillin, and 100 mg/mL streptomycin antibiotics (GIBCO). Culture conditions were 37 °C with 5% CO_2 and 5% O_2. Cells were passaged when 80–90% confluent. *Myotis myotis* primary fibroblasts were obtained from collaborators who generated and expanded from non-lethally sampled 3 mm wing biopsies using methods detailed in ref. 1. At least three individuals of each species were sampled, generating independent cell lines. Cells with PD lower than 30 were used for all experiments. Population doubling was calculated using the formula: [3.32*log (cell number harvested - cell number seeded)] + PD of cells seeded.

To isolate kidney epithelial cells, kidneys were minced and digested with Liberase™ at 37 °C for 30 min. Digested tissue was strained using a 100 µm cell strainer, and clumps were pressed using a syringe plunger. Cells were pelleted and incubated in 1× RBC lysis buffer for 10 min in the dark with occasional shaking. Following a wash with PBS, cells were plated and grown in DMEM with 10 % FBS, 1X Antibiotic-Antimycotic, and 1× Primocin (InvivoGen). Generally, fibroblasts are easily detached during trypsinization when compared to cuboidal epithelial cells. Fibroblast contamination was minimized by a short trypsinization and discard of detached cells during regular passaging.

Telomerase repeated amplification protocol (TRAP)

TRAP assay was performed using the TRAPeze kit (Cat. #S7700, Millipore Sigma). Briefly, 0.5 million cells were resuspended in CHAPs lysis buffer, and the amount of protein was estimated using Pierce BCA Protein Assay Kits (Cat. # 23225, Thermo Fisher Scientific). TRAP assay was performed using 250 ng of cell extracts, and the manufacturer's instructions were followed. HeLa cell lysates were used as positive controls. Uncropped gel images are provided in the Source Data file.

Soft agar assay

Following plasmids were used in this assay to generate stable cell lines: pCMV-HRas^{G12V} (Clontech), Piggyback vectors, pPB-SV40 LT, pPB-SV40 LT-K1, pPB-SV40 LT- Δ434-444, pBase, GFP control (Launchpad AVA2590, plasmid #85442). Cells were transfected using Amaxa nucleofector (Lonza) using the manufacturer's protocol T-20. Stable cell lines were generated using puromycin (0.25-0.5 µg/mL) or hygromycin (25–50 µg/mL), depending on the plasmids and their combinations. For soft agar assay, 2X complete medium was prepared using 2X EMEM, 30% FBS, and 2X antibiotics as required. A base layer was poured into plates after mixing with 1% agarose (Difco Agar Noble). The top layer was made similarly, where 2X complete medium was mixed with 0.8% agarose and 10,000 cells/35 mm well and layered on top of the base layer. Following the solidification of agarose, 1 mL 1X complete media with antibiotics was added on top and refurbished twice a week. Plates were incubated at 37 °C in a humidified incubator for three weeks. Plates were then imaged for colonies in soft agar.

Xenograft assay

Animal experiments were performed under pre-approved protocols and in accordance with guidelines set by the University of Rochester Committee on Animal Resources (UCAR). Fibroblasts stably expressing oncogenes or a combination of oncogenes were tested for tumor formation in female NIH III nude mice (Charles River, Crl:NIH-Lystbg-JFoxn1nuBtkxid). Mice were 3–8 weeks of age and were kept under specific pathogen-free (SPF) conditions at the vivarium of the University of Rochester. Mice were housed in 12 h light/ 12 h dark cycle, at temperatures 18–23 C, with 40–60% humidity. Each flank of the nude mice was injected with two million cells in 100 µL PBS mixed with an equal volume of Matrigel using a 22-gauge needle. A total of 8 injections per cell line were tested. Tumor formation was monitored twice a week, and dimensions were measured using Vernier calipers. As per UCAR guidelines, a tumor long diameter <5 mm was considered negative, and 20 mm was considered the tumor burden endpoint. Maximal tumor burden was not exceeded. Mice that did not reach tumor burden endpoints were terminated after a maximum of 60 days. Euthanized mice were photographed, and tumors were excised, photographed, weighed, frozen at −80 °C, and preserved in formalin.

Gamma-radiation and Nutlin-3 treatments

Radiation treatment was performed using a γ-radiator (Model 8114 Shepherd Cs^{137}). Cells were seeded 24–48 h before treatments. Following treatment with radiation doses 10 and 20 Gy, the cell culture medium was immediately changed, and cells were returned to the incubator.

For induction of senescence, radiated cells were incubated for 12 days, and the culture medium was replaced twice a week. For Nutlin-3 (CAS 548472-68-0, Santa Cruz) treatment, different concentrations of Nutlin-3 (10 and 50 µM) in DMSO were added to cells and incubated for 24 h for apoptosis assay or 6 h for western blotting.

BrdU incorporation assay

Cells were seeded 24 h before treatment and were allowed to grow in the presence of 3 µg/mL BrdU (BD Pharmingen) for 48 h. Cells were trypsinized and fixed with 70% cold ethanol for 30 min. For staining, fixed cells were washed twice with PBS and treated with 2 N HCl for 30 min for DNA denaturation. Following two more PBS washes, cells were incubated with 5% BSA for 1 h at room temperature (RT). Cells were then incubated with anti-BrdU (Alexa Fluor® 647 Mouse anti-BrdU, Clone 3D4 (RUO)) antibody overnight at 4 °C. Following 2 × PBS washes, stained cells were analyzed by flow cytometry with appropriate positive and negative controls. Gating for flow cytometry was set using negative control cells (Supplementary Fig. 3b).

Apoptosis assay

Apoptosis assay was performed using Annexin V FLUOS staining kit (Roche), and the manufacturer's instructions were followed with slight modifications. Briefly, culture supernatant and PBS washes were collected. Cells were then trypsinized briefly, and the cell pellet was mixed with the floating cells collected from the supernatant and washes. Following two more washes with PBS, the cell pellet was resuspended in Annexin-V-FLUOS labeling reagent containing Annexin V and propidium iodide. Following a 10 min incubation on ice, cells were immediately analyzed by flow cytometry with appropriate positive and negative controls. Samples from each replicate were analyzed using gates set with untreated controls of that replicate (Supplementary Fig. 3a).

Senescence-associated β-gal staining

Irradiated cells were incubated for 12 days, and the media was replaced twice a week. After 12 days, approximately 24–48 h before staining, cells were seeded to be approximately 40% confluent. Cells were washed 2X with PBS and fixed for 5 min with 2% formaldehyde. Cells were washed gently to remove formaldehyde and staining solution (1 mg/ml X-gal in DMSO, 40 mM Citric acid/Sodium phosphate buffer pH 6, 5 mM potassium ferricyanide, 5 mM potassium ferricyanide, 150 mM NaCl, 2 mM $MgCl_2$) was added to the cells. Cells were incubated for 12–24 h at 37 °C. Following the development of blue color, cells were washed 2X with PBS, overlayed with 70% glycerol, and imaged. Cells were counted under the light microscope, and the percentage of SA-β-gal positive cells was determined.

Plasmid luciferase reporter assay

Cells were seeded in 24-well plates 24 h before transfection. Following manufacturers' instructions, about 250–300 ng of plasmids were transfected using Fugene (Invitrogen). p53-TA-Luc (Clontech/Takara) was used to assay p53 transcriptional activity, and pRL-CMV (Promega) was used as the transfection control. Reporter activity was analyzed 48 h post-transfection using the Dual luciferase reporter assay system and the GloMax 20/20 Luminometer (Promega). Manufacturers' instructions were followed, and activity ratios are reported as relative luciferase units (RLU).

RNA sequencing (RNA-seq)

Total RNA was extracted from irradiated or non-irradiated fibroblasts from four bat species, laboratory mice, wild-caught mice, and humans using PureLink™ RNA Mini Kit (Thermo Fisher Scientific) following the manufacturer's instructions. NGS-TruSeq Stranded mRNA libraries were generated and sequenced with Illumina NovaSeq 6000 single-end 75 bp sequencing at the University of Rochester Genomics Research Center. Whole skin tissue transcriptome was generated from three species of bats – *E. fuscus* (4 individuals), and *A. jamaicensis* (3 individuals), and *E. spelaea* (5 individuals).

Genome assembly, annotation, and gene expression analysis

Raw reads were demultiplexed using conFig.bcl2fastq.pl (v1.8.4). Adapter sequences and low-quality base calls (threshold: Phred quality score < 20) in the RNA-seq reads were first trimmed using Fastp (0.23.4)[84]. For all species, the clean reads were aligned using Salmon (v1.5.1)[85] to the longest coding sequence (CDS) of each gene extracted from the corresponding genome assembly based on genome

annotations using GffRead (v0.12.7)[86]. The genome assemblies used in this study include GCA_003508835.1 (*Eonycteris spelaea*), EptFus1.0_HiC (DNA Zoo Consortium, *Eptesicus fuscus*), GCA_004027435.1 (*Artibeus jamaicensis*), Myoluc2.0_HiC (DNA Zoo Consortium, *Myotis lucifugus*), GCF_000001635.27 (*Mus musculus*), and GCA_000001405.29 (*Homo sapiens*). Human-referenced TOGA annotations were used when the original genomic annotations are not available[87]. The orthologous genes of each species to human reference were identified by performing a reciprocal blast search (BLAST + v2.10.1)[88] against human longest protein (GRCh38.p13; Ensembl database, release109) with parameters of "-evalue 1e-05; -max_target_seqs 1", and hits with query coverage > 30% were retained. The values of read count and effective gene lengths for each gene were collected and integrated into gene-sample table according to their orthologous relationship. Salmon transcript counts were used to perform differential expression analysis. Only human genes with orthologs in all species were kept for the downstream analysis. To filter out low-expressed genes, only genes with all sample read counts sum > 10 was retained. The filtered count matrix was normalized using the median of ratios method[89] implemented in DESeq2 package (v1.40.2)[90]. Since orthologous gene lengths could vary among different species, we implemented an additional length normalization step in the DESeq2 pipeline to avoid biased comparative quantifications resulting from species-specific transcript length variations. To do this, the matrix of effective lengths for each gene in each sample was delivered to the DESeq2 'DESeqDataSet' object so that they are included in the normalization for downstream analysis. Differential expression analysis, using either irradiated cells (24 h or 12 days) versus control (24 h or 12 days) or only irradiated cells from 24 h versus 12 days in each species, was performed using DESeq2. We considered all differentially expressed genes (DEGs) with an adjusted $p < 0.05$, and 1.5-fold expression change to be statistically significant in our analyses.

Functional enrichment analysis

Hallmark gene sets and C2 curated gene sets from MsigDB were used for GSEA analysis using the ranked fold changes from the DEG analysis. The *p*-values were calculated using a permutation-based approach. For cellular senescence analysis, in addition to MsigDB gene sets, we also collected gene sets identified as the senescence signature using transcriptomic and proteomic approaches from published literature[44–46]. For NK cell transcriptional signature GSEA analysis in skin tissue transcriptome, bulk RNA-seq data from tissues of bats and rat, mice and naked mole rats[78] and NK cell-related transcriptomes reported in published studies and MsigDB[79–81] were used.

Batch analysis of TP53 copy number in bat genomes

BLAST was used to search for *TP53* genes in bats genomes using the human TP53 protein

sequence as a query. The best-matched genomic regions plus 5 kb up- and downstream flanking

sequences were extracted from the genome for GeneWise[91] gene structure prediction. Predicted genes with more than 80% coverage of the human TP53 protein were treated as TP53 duplicates. To further confirm that the identified TP53 copies in *M. lucifugus* are not misidentified homologs from the TP53 gene family, additional blast analysis with human TP63 and TP73 was performed. Promoter prediction in − 20 kb upstream sequence of the TP53 gene was performed using Promoter 2.0 (https://services.healthtech.dtu.dk/services/Promoter-2.0/)[92]. The predicted promoters with score > 1 were considered as high-confidence promoters.

TP53 copy number analysis in *M. lucifugus* genome

BLAST was used to search for *TP53* genes in bats genomes using the human TP53 protein sequences as a query. The best matched genomic regions plus 5 kb up- and downstream flanking sequence were extracted from the genome for GeneWise gene structure prediction. Predicted genes with more than 80% converge of human TP53 protein were treated as the *TP53* duplicates. To confirm that the identified *TP53* copies in *M. lucifugus* are not misidentified homologs from the p53 gene family, additional blast analysis with human *TP63* and *TP73* was performed.

Cas9 targeted sequencing

High molecular weight (HMW) genomic DNA from a single *M. lucifugus* fibroblast line was isolated using the Nanobind ®HMW DNA extraction kit for cultured cells (PacBio). *M. lucifugus* TP53 copy sequences found in the Myoluc2.0 genome assembly were used to design guide RNAs (listed in Supplementary Table 2) using Benchling. Guides were designed to cut within sequences of TP53 gene copies and sequence across part of the gene into flanking regions. The Cas9 Sequencing Kit SQK-CS9109 (Oxford Nanopore Technologies) was used for targeted sequencing according to the manufacturer protocol. Briefly, extracted HMW gDNA was phosphatase-treated to remove pre-existing phosphorylated ends, followed by heat inactivation. Next, target regions were cleaved in vitro using Cas9 ribonucleoprotein complexes consisting of Alt-R® S.p. HiFi Cas9 Nuclease V3 (Integrated DNA Technologies), Alt-R® CRISPR-Cas9 tracRNA (Integrated DNA Technologies), and target-specific Alt-R® CRISPR-Cas9 crRNAs (Integrated DNA Technologies). Following cleavage, Cas9 was heat-inactivated, and adapters were ligated to the cleaved phosphorylated ends. Adapters from Ligation Sequencing Kit V14 SQK-LSK114 (Oxford Nanopore Technologies) were used in place of the adapter included in the Cas9 kit. Following adapter ligation, samples were cleaned up using AMPure XP Beads and loaded onto a R10.4.1 flow cell on a MinION Mk1C (Oxford Nanopore Technologies) for sequencing. Raw data was base-called in Super-High accuracy mode and aligned to *M. lucifugus* TP53 reference sequences in both Guppy and Dorado with read splitting enabled. The list of guides used is shown in Supplementary Table 2.

Statistics & reproducibility

GraphPad Prism 10 was used to generate graphs and for statistical analysis for all data, excluding RNA-seq analysis. Error bars show standard deviation (SD). Two-tailed Student's *t* test was used to test the statistical significance of the differences between groups unless otherwise indicated. $P < 0.05$ was set as a threshold for statistical significance. Experiments were reproducible with at least 3 independent biological replicates. No statistical method was used to predetermine sample size, no blinding or randomization were used.

Reporting summary

Further information on research design is available in the Nature Portfolio Reporting Summary linked to this article.

Data availability

The raw RNA sequencing data of all bat fibroblasts and tissues are available in the Gene Expression Omnibus (GEO) under accession: GSE262772. The Cas9-targeted sequencing data is available in NCBI-SRA under accession number PRJNA1252734. The data generated in this study are provided in the Source Data file. The exact P values, if applicable, are included in the paper and in the Source Data. Source data are provided with this paper. The remaining data are available within the Article, Supplementary Information, or Source Data file. Source data are provided in this paper.

References

1. Foley, N. M. et al. Growing old, yet staying young: The role of telomeres in bats' exceptional longevity. *Sci. Adv.* **4**, eaao0926 (2018).
2. Sadier, A. et al. Making a bat: The developmental basis of bat evolution. *Genet. Mol. Biol.* **43**, e20190146 (2021).

3. Wilkinson, G. S. & Adams, D. M. Recurrent evolution of extreme longevity in bats. *Biol. Lett.* **15**, 20180860 (2019).
4. Peto, R. Quantitative implications of the approximate irrelevance of mammalian body size and lifespan to lifelong cancer risk. *Philos. Trans. R Soc. Lond. B Biol. Sci.* **370**, https://doi.org/10.1098/rstb.2015.0198 (2015).
5. Compton, Z. T. et al. Cancer prevalence across vertebrates. *Cancer Discov.* ***15***, 227–244 (2023).
6. Vincze, O. et al. Cancer risk across mammals. *Nature* **601**, 263–267 (2022).
7. Bulls, S. E. et al. Unraveling the relationship between cancer and life history traits in vertebrates. Preprint at https://doi.org/10.1101/2022.07.12.499088 (2024).
8. Berben, L. et al. Cancer and aging: Two tightly interconnected biological processes. *Cancers* **13**, https://doi.org/10.3390/cancers13061400 (2021).
9. Armitage, P. & Doll, R. The age distribution of cancer and a multi-stage theory of carcinogenesis. *Br. J. Cancer* **91**, 1983–1989 (2004).
10. Siegal-Willott, J. et al. Microchip-associated leiomyosarcoma in an Egyptian fruit bat (Rousettus aegyptiacus). *J. Zoo. Wildl. Med.* **38**, 352–356 (2007).
11. Bradford, C., Jennings, R. & Ramos-Vara, J. Gastrointestinal leiomyosarcoma in an Egyptian fruit bat (Rousettus aegyptiacus). *J. Vet. Diagn. Invest.* **22**, 462–465 (2010).
12. McLelland, D. J., Dutton, C. J. & Barker, I. K. Sarcomatoid carcinoma in the lung of an Egyptian fruit bat (Rousettus aegyptiacus). *J. Vet. Diagn. Invest.* **21**, 160–163 (2009).
13. Pace, C. et al. A review of neoplasms in a population of Jamaican fruit bats (Artibeus Jamaicensis) under human care. *J. Zoo. Wildl. Med.* **53**, 583–592 (2022).
14. Seluanov, A. et al. Telomerase activity coevolves with body mass not lifespan. *Aging Cell* **6**, 45–52 (2007).
15. Tian, X. et al. Evolution of telomere maintenance and tumour suppressor mechanisms across mammals. *Philos. Trans. R Soc. Lond. B Biol. Sci.* **373**, https://doi.org/10.1098/rstb.2016.0443 (2018).
16. Gomes, N. M. et al. Comparative biology of mammalian telomeres: hypotheses on ancestral states and the roles of telomeres in longevity determination. *Aging Cell* **10**, 761–768 (2011).
17. Abegglen, L. M. et al. Potential mechanisms for cancer resistance in elephants and comparative cellular response to DNA damage in humans. *JAMA* **314**, 1850–1860 (2015).
18. Sulak, M. et al. TP53 copy number expansion is associated with the evolution of increased body size and an enhanced DNA damage response in elephants. *Elife* **5**, https://doi.org/10.7554/elife.11994 (2016).
19. Vazquez, J. M. and Lynch, V. J. Pervasive duplication of tumor suppressors in Afrotherians during the evolution of large bodies and reduced cancer risk. *Elife* **10**, https://doi.org/10.7554/elife.65041 (2021).
20. Ricci, M. et al. Comparative analysis of bats and rodents' genomes suggests a relation between non-LTR retrotransposons, cancer incidence, and ageing. *Sci. Rep.* **13**, 9039 (2023).
21. Zhao, Y. et al. Transposon-triggered innate immune response confers cancer resistance to the blind mole rat. *Nat. Immunol.* **22**, 1219–1230 (2021).
22. Tian, X. et al. SIRT6 Is responsible for more efficient DNA double-strand break repair in long-lived species. *Cell* **177**, 622–638 (2019).
23. Gorbunova, V. et al. Cancer resistance in the blind mole rat is mediated by concerted necrotic cell death mechanism. *Proc. Natl. Acad. Sci. USA* **109**, 19392–19396 (2012).
24. Seluanov, A. et al. Hypersensitivity to contact inhibition provides a clue to cancer resistance of naked mole-rat. *Proc. Natl. Acad. Sci. USA* **106**, 19352–19357 (2009).
25. Zhang, G. et al. Comparative analysis of bat genomes provides insight into the evolution of flight and immunity. *Science* **339**, 456–460 (2013).
26. Escalera-Zamudio, M. et al. The evolution of bat nucleic acid-sensing Toll-like receptors. *Mol. Ecol.* **24**, 5899–5909 (2015).
27. Pavlovich, S. S. et al. The Egyptian Rousette genome reveals unexpected features of bat antiviral immunity. *Cell* **173**, 1098–1110 (2018).
28. Zepeda Mendoza, M. L. et al. Hologenomic adaptations underlying the evolution of sanguivory in the common vampire bat. *Nat. Ecol. Evol.* **2**, 659–668 (2018).
29. Hawkins, J. A. et al. A metaanalysis of bat phylogenetics and positive selection based on genomes and transcriptomes from 18 species. *Proc. Natl. Acad. Sci. USA* **116**, 11351–11360 (2019).
30. Jebb, D. et al. Six reference-quality genomes reveal evolution of bat adaptations. *Nature* **583**, 578–584 (2020).
31. Irving, A. T. et al. Lessons from the host defences of bats, a unique viral reservoir. *Nature* **589**, 363–370 (2021).
32. Moreno Santillan, D. D. et al. Large-scale genome sampling reveals unique immunity and metabolic adaptations in bats. *Mol. Ecol.* **30**, 6449–6467 (2021).
33. Vazquez, J. M. et al. Extensive longevity and DNA virus-driven adaptation in Nearctic Myotis bats. Preprint at https://doi.org/10.1101/2024.10.10.617725 (2024).
34. Gorbunova, V., Seluanov, A. & Kennedy, B. K. The world goes bats: Living longer and tolerating viruses. *Cell Metab.* **32**, 31–43 (2020).
35. Scheben, A. et al. Long-read sequencing reveals rapid evolution of immunity- and cancer-related genes in bats. *Genome Biol. Evol.* **15**, https://doi.org/10.1093/gbe/evad148 (2023).
36. Seim, I. et al. Genome analysis reveals insights into physiology and longevity of the Brandt's bat Myotis brandtii. *Nat. Commun.* **4**, 2212 (2013).
37. Hua, R. et al. Experimental evidence for cancer resistance in a bat species. *Nat. Commun.* **15**, 1401 (2024).
38. Rangarajan, A. et al. Species- and cell type-specific requirements for cellular transformation. *Cancer Cell* **6**, 171–183 (2004).
39. Teeling, E. C. et al. A molecular phylogeny for bats illuminates biogeography and the fossil record. *Science* **307**, 580–584 (2005).
40. Gorbunova, V. & Seluanov, A. Coevolution of telomerase activity and body mass in mammals: from mice to beavers. *Mech. Ageing Dev.* **130**, 3–9 (2009).
41. Gorbunova, V. et al. Comparative genetics of longevity and cancer: insights from long-lived rodents. *Nat. Rev. Genet.* **15**, 531–540 (2014).
42. Borghesan, M. et al. A senescence-centric view of aging: Implications for longevity and disease. *Trends Cell Biol.* **30**, 777–791 (2020).
43. Kuilman, T. et al. The essence of senescence. *Genes Dev.* **24**, 2463–2479 (2010).
44. Saul, D. et al. A new gene set identifies senescent cells and predicts senescence-associated pathways across tissues. *Nat. Commun.* **13**, 4827 (2022).
45. Basisty, N. et al. A proteomic atlas of senescence-associated secretomes for aging biomarker development. *PLoS Biol.* **18**, e3000599 (2020).
46. Hernandez-Segura, A. et al. Unmasking transcriptional heterogeneity in senescent cells. *Curr. Biol.* **27**, 2652–2660 (2017).
47. Miyashita, T. & Reed, J. C. Tumor suppressor p53 is a direct transcriptional activator of the human bax gene. *Cell* **80**, 293–299 (1995).
48. Shi, D. & Gu, W. Dual Roles of MDM2 in the Regulation of p53: Ubiquitination Dependent and Ubiquitination Independent Mechanisms of MDM2 Repression of p53 Activity. *Genes Cancer* **3**, 240–248 (2012).

49. Kung, C. P. & Weber, J. D. It's getting complicated-A fresh look at p53-MDM2-ARF triangle in tumorigenesis and cancer therapy. *Front. Cell Dev. Biol.* **10**, 818744 (2022).
50. Farnebo, M. Wrap53, a novel regulator of p53. *Cell Cycle* **8**, 2343–2346 (2009).
51. Mahmoudi, S. et al. Wrap53, a natural p53 antisense transcript required for p53 induction upon DNA damage. *Mol. Cell* **33**, 462–471 (2009).
52. Huang, Z. et al. Longitudinal comparative transcriptomics reveals unique mechanisms underlying extended healthspan in bats. *Nat. Ecol. Evol.* **3**, 1110–1120 (2019).
53. Nishiyama, H. et al. A glycine-rich RNA-binding protein mediating cold-inducible suppression of mammalian cell growth. *J. Cell Biol.* **137**, 899–908 (1997).
54. Padariya, M. et al. The elephant evolved p53 isoforms that escape MDM2-mediated repression and cancer. *Mol. Biol. Evol.* **39**, https://doi.org/10.1093/molbev/msac149 (2022).
55. Dudchenko, O. et al. De novo assembly of the Aedes aegypti genome using Hi-C yields chromosome-length scaffolds. *Science* **356**, 92–95 (2017).
56. Lindblad-Toh, K. et al. A high-resolution map of human evolutionary constraint using 29 mammals. *Nature* **478**, 476–482 (2011).
57. Shay, J. W. Role of telomeres and telomerase in aging and cancer. *Cancer Discov.* **6**, 584–593 (2016).
58. Coppe, J. P. et al. Senescence-associated secretory phenotypes reveal cell-nonautonomous functions of oncogenic RAS and the p53 tumor suppressor. *PLoS Biol.* **6**, 2853–2868 (2008).
59. Coppe, J. P. et al. The senescence-associated secretory phenotype: the dark side of tumor suppression. *Annu. Rev. Pathol.* **5**, 99–118 (2010).
60. Banerjee, A. et al. Lack of inflammatory gene expression in bats: a unique role for a transcription repressor. *Sci. Rep.* **7**, 2232 (2017).
61. Zhou, P. et al. Contraction of the type I IFN locus and unusual constitutive expression of IFN-alpha in bats. *Proc. Natl. Acad. Sci. USA* **113**, 2696–2701 (2016).
62. Vogelstein, B., Lane, D. & Levine, A. J. Surfing the p53 network. *Nature* **408**, 307–310 (2000).
63. Menendez, D., Inga, A. & Resnick, M. A. The expanding universe of p53 targets. *Nat. Rev. Cancer* **9**, 724–737 (2009).
64. Malonia, S. K. et al. F-box protein FBXO31 directs degradation of MDM2 to facilitate p53-mediated growth arrest following genotoxic stress. *Proc. Natl. Acad. Sci. USA* **112**, 8632–8637 (2015).
65. Caulin, A. F. et al. Solutions to Peto's paradox revealed by mathematical modelling and cross-species cancer gene analysis. *Philos. Trans. R Soc. Lond. B Biol. Sci.* **370**, https://doi.org/10.1098/rstb.2014.0222 (2015).
66. Garcia-Cao, I. et al. Super p53" mice exhibit enhanced DNA damage response, are tumor resistant and age normally. *EMBO J.* **21**, 6225–6235 (2002).
67. Tyner, S. D. et al. p53 mutant mice that display early ageing-associated phenotypes. *Nature* **415**, 45–53 (2002).
68. Dang, C. V. A metabolic perspective of Peto's paradox and cancer. *Philos. Trans. R Soc. Lond. B Biol. Sci.* **370**, https://doi.org/10.1098/rstb.2014.0223 (2015).
69. Brunet-Rossinni, A. K. Reduced free-radical production and extreme longevity in the little brown bat (Myotis lucifugus) versus two non-flying mammals. *Mech. Ageing Dev.* **125**, 11–20 (2004).
70. O'Mara, M. T. et al. Cyclic bouts of extreme bradycardia counteract the high metabolism of frugivorous bats. *Elife* **6**, https://doi.org/10.7554/elife.26686 (2017).
71. Chionh, Y. T. et al. High basal heat-shock protein expression in bats confers resistance to cellular heat/oxidative stress. *Cell Stress Chaperones* **24**, 835–849 (2019).
72. Koh, J. et al. ABCB1 protects bat cells from DNA damage induced by genotoxic compounds. *Nat. Commun.* **10**, 2820 (2019).
73. Salmon, A. B. et al. The long lifespan of two bat species is correlated with resistance to protein oxidation and enhanced protein homeostasis. *FASEB J.* **23**, 2317–2326 (2009).
74. Zhao, H. et al. Inflammation and tumor progression: signaling pathways and targeted intervention. *Signal Transduct. Target Ther.* **6**, 263 (2021).
75. Aso, H. et al. Single-cell transcriptome analysis illuminating the characteristics of species-specific innate immune responses against viral infections. *Gigascience* **12**, https://doi.org/10.1093/gigascience/giad086 (2022).
76. Friedrichs, V. et al. Landscape and age dynamics of immune cells in the Egyptian rousette bat. *Cell Rep.* **40**, 111305 (2022).
77. Ren, L. et al. Single-cell transcriptional atlas of the Chinese horseshoe bat Rhinolophus sinicus provides insight into the cellular mechanisms which enable bats to be viral reservoirs. Preprint at https://doi.org/10.1101/2020.06.30.175778 (2020).
78. Lu, J. Y. et al. Comparative transcriptomics reveals circadian and pluripotency networks as two pillars of longevity regulation. *Cell Metab.* **34**, 836–856 (2022).
79. Costanzo, M. C. et al. Transcriptomic signatures of NK cells suggest impaired responsiveness in HIV-1 infection and increased activity post-vaccination. *Nat. Commun.* **9**, 1212 (2018).
80. Wu, M. et al. Comprehensive characterization of tumor infiltrating natural killer cells and clinical significance in hepatocellular carcinoma based on gene expression profiles. *Biomed. Pharmacother.* **121**, 109637 (2020).
81. Mobus, L. et al. Elevated NK-cell transcriptional signature and dysbalance of resting and activated NK cells in atopic dermatitis. *J. Allergy Clin. Immunol.* **147**, 1959–1965 (2021).
82. de Magalhaes, J. P. et al. Human ageing genomic resources: updates on key databases in ageing research. *Nucleic Acids Res.* **52**, D900–D908 (2024).
83. Seluanov, A., Vaidya, A. & Gorbunova, V. Establishing primary adult fibroblast cultures from rodents. *J. Vis. Exp.* **44**, https://doi.org/10.3791/2033 (2010).
84. Chen, S. et al. fastp: an ultra-fast all-in-one FASTQ preprocessor. *Bioinformatics* **34**, i884–i890 (2018).
85. Patro, R. et al. Salmon provides fast and bias-aware quantification of transcript expression. *Nat. Methods* **14**, 417–419 (2017).
86. Pertea, G. & Pertea, M. GFF Utilities: GffRead and GffCompare. *F1000Res.* **9**, https://doi.org/10.12688/f1000research.23297.2 (2020).
87. Kirilenko, B. M. et al. Integrating gene annotation with orthology inference at scale. *Science* **380**, eabn3107 (2023). p.
88. Camacho, C. et al. BLAST+: architecture and applications. *BMC Bioinform.* **10**, 421 (2009).
89. Anders, S. & Huber, W. Differential expression analysis for sequence count data. *Genome Biol.* **11**, R106 (2010).
90. Love, M. I., Huber, W. & Anders, S. Moderated estimation of fold change and dispersion for RNA-seq data with DESeq2. *Genome Biol.* **15**, 550 (2014).
91. Birney, E., Clamp, M. & Durbin, R. GeneWise and genomewise. *Genome Res.* **14**, 988–995 (2004).
92. Knudsen, S. Promoter2.0: for the recognition of PolII promoter sequences. *Bioinformatics* **15**, 356–361 (1999).

Acknowledgements

We thank Julia Ablaeva, Anatoly Korotkov, and Syed Ali Biashad at the University of Rochester for help with the collection of bat tissues and isolation of primary fibroblasts. We thank Richard Miller for generously providing *Myotis lucifugus* fibroblasts. We thank Randy Foo for providing technical assistance with bat colony management at Duke-NUS and providing bat tissues for this study. The work at Duke-NUS is funded by grants from the Singapore National Research Foundation (NRF-CRP10-2012-05), National Medical Research Council

(OFIRG19nov-0050), and Ministry of Education (MOE2019-T2-2-130). This study was supported by grants from the National Institute on Aging to VG and AS, and grants from the Michael Antonov Foundation and Milky Way Research Foundation to VG and from a Science Foundation Future Frontiers (grant no. 19/FFP/6790) awarded to ECT.

Author contributions

Designed experiments: F.A., A.S., and V.G.; Performed experiments: F.A.; Bioinformatic analysis: Z.Z., S.R., and J.Y.L.; Assisted with experiments: M.Z., Y.Z., and V.V.; Contributed research materials: D.A., A.G., L.N.C., T.S., L.W., and E.C.T.; Data interpretation: F.A., Z.Z., S.R., E.C.T, A.S., and V.G.; Wrote manuscript: F.A., Z.Z., E.C.T., A.S., and V.G. All authors read and approved the manuscript.

Competing interests

L.W. and E.C.T. serve on the scientific advisory board of Paratus Sciences, a company developing the tools and methods necessary to understand bat biology and apply these insights to develop new therapies. Other authors declare no competing interests.

Additional information

Supplementary information The online version contains supplementary material available at https://doi.org/10.1038/s41467-025-59403-z.

Correspondence and requests for materials should be addressed to Andrei Seluanov or Vera Gorbunova.

Peer review information *Nature Communications* thanks Zachary Compton, Vadim Fraifeld who co-reviewed with Ekaterina RudnitskyHuabin Zhao and Shaying Zhao for their contribution to the peer review of this work. A peer review file is available.